Tutor/s

Dr. Alejandro Pérez Rodriguez
Departament Electrònica

Dr. Edgardo Saucedo
IREC

UNIVERSITAT DE BARCELONA

Grau d'Enginyeria de Materials

Treball Final de Grau

Exploring the dynamic of Sn for the synthesis of high efficiency $Cu_2ZnSnSe_4$ based solar cells.

Explorando la dinámica del Sn durante la síntesis de celdas de alta eficiencia basadas en $Cu_2ZnSnSe_4$.

Alejandro Navarro Güell

Julio 2020

UNIVERSITAT DE BARCELONA

Dos campus d'excel·lència internacional

B:KC Barcelona Knowledge Campus

HUB Health Universitat de Barcelona Campus

Daria todo lo que sé, por la mitad de lo que ignoro.

Renè Descartes

Agradecimientos:

Gracias al Dr. Alejandro Pérez por ofrecer la oportunidad de hacer el TFG con ellos en IREC.

Gracias al Dr. Edgardo por haber confiado en mí y haberme ayudado en todo momento.

Gracias al Dr. Kunal Tiwari por haber ser un compañero excelente y haberme enseñado a trabajar en el laboratorio.

Gracias al Dr. Ignacio Becerril por haber respondido mis cientos de preguntas y por todas las explicaciones que me ha dado.

Gracias al Dr. Jacob Andrade por haberme enseñado a ser un mejor investigador.

Gracias a la Dra. Yudania Sánchez por el apoyo y la ayuda.

Gracias a Alex y a Pedro por haber estado ahí cuando les he necesitado.

En general gracias a todo el equipo Solar que me ha hecho sentir como uno más en IREC.

A Judith Fuentes Llanos por toda su ayuda y por su apoyo moral.

REPORT

CONTENTS

1. GLOSSARY

a-Si:	Amorphous Silicon
CB:	Conduction Band
c-Si:	Crystalline Silicon
CIG(S,Se):	Copper-Indium-Galium-(Sulphur, Selenide)
CVD:	Chemical Vapour Deposition
E_g:	Bandgap Energy
FF:	Fill Factor
GHG:	Greenhouse Gases
I_0:	Dark Saturation Current
I_L:	Light generated current
I_{sc}:	Short-Circuit current
$I_{MP:}$	Maximum current
ITO:	Indium-Tin Oxide
$K_{b:}$	Boltzmann Constant
η = PCE:	Power Conversion Efficiency
n:	Electrons concentration
n_i:	Intrinsic semiconductor carrier concentration
OPD:	Organic Photovoltaic Device
p:	Holes concentration
p-Si:	Polycrystalline Silicon
PSC:	Perovskite Solar Cell
PLD:	Pulsed Laser Deposition

PVD: Physical Vapour Deposition

PV: Photovoltaics

QE: Quantum Efficiency

R_{sh}: Shunt Resistance

R_s: Series Resistance

SCR: Space Charge Region

SLG: Soda-Lime Glass

STC: Standard Test Conditions

TCO: Transparent Conducting Oxide

T: Temperature

VB: Valence Band

V_{oc}: Open-Circuit voltage

V_{MP}: Maximum voltage

XRD: X-Ray Diffraction

XRF: X-Ray Fluorescence

2. SUMMARY

The need for new renewable sources of energy has been a reality for several years. Both because our current source of energy, fossil fuels, is limited, and because of the high pollution and problems associated with their use. As a solution to this problem, the development of renewable energies is our best asset. Within the wide range of possibilities, this work focuses on the energy that directly uses the enormous potential of our sun, photovoltaic energy.

One of the most promising materials for emerging applications in the field of photovoltaics are the so-called kesterites, formed by the elements: Cu, Zn, Sn and Se; all of which are abundant and of low or null toxicity. The development of high efficiency cells based on kesterite faces several challenges related to the complex nature of this family of materials. Among them, the control of Sn that tends to form liquid and volatile species during the synthesis process having a strong exchange with the annealing atmosphere.

In this work, the dynamics of Sn during the synthesis of the photovoltaic absorber, $Cu_2ZnSnSe_4$ (CZTSe), is investigated through a sequential process (Sputtering + Annealing). We compare the classical methodology where Sn is already incorporated in the solid precursor with a new and innovative solution in which Sn is partially incorporated in the vapour phase. The impact on the mechanism of CZTSe formation is investigated, as well as the properties of the layers and the characteristics of the finished devices.

3. RESUMEN

La necesidad de disponer de nuevas fuentes de energía renovable es una realidad desde hace ya unos cuantos años. Tanto porque nuestra fuente actual de energía, los combustibles fósiles, son limitados como por la elevada contaminación y problemas que conlleva su utilización. Como solución a este problema, el desarrollo de energías renovables es nuestra mejor baza. Dentro del gran abanico de posibilidades, este trabajo se centra en la energía que utiliza directamente el enorme potencial de nuestro sol, la energía fotovoltaica.

Uno de los materiales más prometedores para las aplicaciones emergentes en el campo de la fotovoltaica son las llamadas kesteritas, formadas por los elementos: Cu, Zn, Sn y Se; todos ellos abundantes y de baja o nula toxicidad. El desarrollo de celdas de alta eficiencia basadas en kesterita se enfrenta a números desafíos relacionados con la compleja naturaleza de esta familia de materiales. Entre ellos, el control del Sn que tiene a formar especies líquidas y volátiles durante el proceso de síntesis sufriendo un gran intercambio con la atmosfera reactiva.

En este trabajo se investiga la dinámica del Sn durante la síntesis del absorbedor fotovoltaico, Cu2ZnSnSe4 (CZTSe), mediante un proceso secuencial (Sputtering + Annealing). Se compara la metodología clásica donde el Sn ya está previamente incorporado en el precursor sólido con una nueva e innovadora solución en la que el Sn se incorpora parcialmente en fase vapor. El impacto provocado en el mecanismo de formación de CZTSe se investiga, así como las propiedades de las capas y las características de los dispositivos terminados.

4. INTRODUCTION

4.1. CLIMATE CHANGE

Climate change is one aspect of the two principal issues concerning the atmospheric damage caused by human activities together with air pollution. These two issues can affect either directly or indirectly. On the one hand the air pollution that affects us directly when breathing which may cause several health problems [1]. On the other hand, probably the biggest problem, is the commonly known Climate change or Global Warming. Nowadays it is well known the devastating effects this change could bring, such as heat waves, disruption of actual stable weather systems, violent weather events such as hurricanes, an increased risk of infectious diseases, threats to food and over time the rising of the sea levels by the melting of polar ice-caps and alpine glaciers [2].

It is clear that the major cause of this problem is the excessive combustion of fossil fuels for energy [3]. Since this is the biggest problem, the most prudent measure includes significant reductions in fossil fuel consumption.

The world's consumption of fossil fuels has increased a 3000% since the beginning of the industrial revolution. While 300 million tonnes were consumed in 1860, this amount increased up to 8730 million tonnes in 1998, and the rate is still increasing.[4].

4.1.1. Greenhouse Effect and GHG

Why is that important to reduce the use of fossil fuels? When part of the Sun's energy is reflected by the earth in the form of infrared radiation, this radiation is absorbed and retained as heat in the lower atmosphere (**Figure 1**). This complex effect is known as greenhouse effect [5]. Gases such as carbon dioxide or water vapor help to retain this heat, thereby stabilizing the Earth's surface temperature. However, due to the increasing rate of oil consumption during the past 100 years, the atmospheric concentration of carbon dioxide has increased by almost 30 percent, rising from 280 ppmv to 360 ppmv.

Other gases in much smaller quantities also contribute to the greenhouse effect. The gases include both naturally originated and others manufactured by humans such as hydrofluorocarbons (HFCs), perfluorocarbons (CFCs) and Sulphur hexafluoride with global warming potentials ranging from 140 to 25000 times greater than CO_2

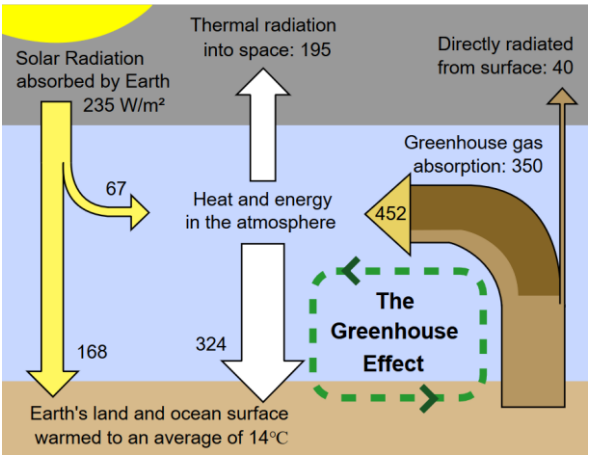

Figure 1: Representation of the Greenhouse effect by Robert A. Rohde

4.1.2. Fossil Fuel Consumption

When we talk about fossil fuels we refer to those that come from biomass produced in passed ages [6]. We can classify them in oil, coal and natural gas. An interesting fact about the formation of fossil fuels is that when a microorganism dies, only about 0.1% of mass escapes, resulting into microbial oxidation within the first centimeters of burial and undergoes anaerobic transformation to fossil fuel.

As a consequence of the previously mentioned, the use of this kind of fuels presents more than one problem. In addition to their polluting and harmful effects, there is the fact that they are not an unlimited resource. The natural formation of these fuels may take several thousand or even millions of years.

Now we are facing the problem that our rate of consumption is much greater than the rate of formation. So, the use of fossil fuels has clearly an ending date, but this date may be too late.

Let's have a quick review of this consumption rate compared to other energy sources using the data provided by bp [7]

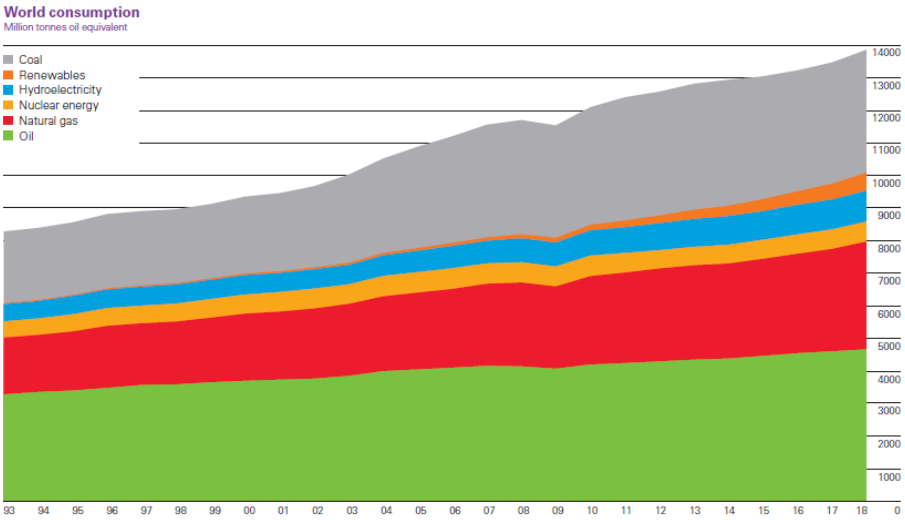

Figure 2: Global energy consumption (Million tonnes oil equivalent per year) [7]

In **Figure 2** we can see how most of the energy comes from fossil fuels leaving behind the astonishing quantity of more than 33 thousand million tonnes of CO2 [7]. At this rate and according to [8], the increase in temperature will pose a serious problem to the world. It is also important to know that because of the time taken to the oceans to warm, we are already committed to substantially more climate change than has ever been experienced. We also must consider that timescales of both atmospheric and human responses are long. All the gases we emit into the atmosphere today will contribute to the increased concentration of those gases and the associated climate change for over 100 years.

With all that in mind it seems clear that we must act immediately.

4.2. Renewable Energy

The field of the renewable energy is probably one of our best shots. The idea of this kind of energy is generating electricity from a virtually inexhaustible source. Fortunately, we have a few options from which we could take advantage, but as we saw in **Figure 2** we are still dependent on non-renewable energies. This fact may be caused by many

factors, from economical interest of the large oil companies to technological problems that we are still investigating.

Another very important characteristic of renewable energies is the fact that they don't emit GHG while operating. This together with the fact that the sources are unlimited makes the renewable energy a much cleaner and prosperous alternative than fossil-fuel based energy. If this wasn't enough, in most parts of the world today, renewables are the lowest-cost source of new power generation, and the costs continue falling every year as we can see in **Table 1**.

Table 1: Global electricity costs in 2018 by IRENA [9]

	Global Weighted-Average Cost of Electricity (USD/kWh) 2018	**Cost of Electricity: 5th and 95th percentiles (USD/kWh)**	**Change in the cost electricity 2017-2018**
Bioenergy	0.062	0.048-0.243	-14%
Geothermal	0.072	0.060-0.143	-1%
Hydro	0.047	0.030-0.136	-11%
Solar photovoltaics	0.085	0.058-0.219	-13%
Concentrating Solar Power	0.185	0.109-0.272	-26%
Offshore wind	0.127	0.102-0.198	-1%
Onshore wind	0.056	0.044-0.100	-13%

In order to have a general idea of the current technologies, following a quick review of the most relevant ones is presented [9]:

- **Wind power**: Differences in pressure and temperature in the atmosphere cause large big masses of air to move, this phenomenon is what we call wind. The wind carries huge amounts of energy that can be transformed by means of large mills that spin turbines thus generating electricity.
- **Geothermal Energy**: Taking profit of the Earth's crust temperature gradient, preferably near zones with volcanic activity, we can heat up water and use once again to spin turbines and generate electricity.
- **Hydropower**: Probably the most used renewable energy source nowadays. It transforms the potential energy of stored water to electricity.
- **Concentrating solar power**: One of the two current alternatives that take advantage of the vast energy provided by the Sun. By concentrating sunlight, it heats up water (or other fluids) and using turbines it generates electricity.

There are some other sources such as bioenergy or marine energy, but they are not of major interest for this Thesis. However, there are a few aspects that are worth noting. Firstly, the primal origin of most of the sources we have already seen is the Sun. Secondly, all of the previous technologies do have the need of using turbines with potent magnets made of not very abundant materials [10].

Now the question that matters is… is there a way of using directly sunlight and converting it into electricity without the need of heating water?

Figure 3: Renewable energy sources

4.3. PHOTOVOLTAIC ENERGY

One of the most promising technologies in the field of renewable energy, and the backbone of this work, is the photovoltaic energy. But before getting started with the main theme of the thesis let's go deeper on the foundations of this interesting way of generating electricity. Let's start from de beginning.

4.3.1. The Photovoltaic Effect

Back in 1839 Edmond Becquerel demonstrated for the first time the photovoltaic effect. This effect is closely related to the photoelectric effect discovered by Albert Einstein. The main difference between these two effects is that whilst the photoelectric ejects an electron when a photon with enough energy is absorbed, in the case of the photovoltaic effect the excited electron or other charge carrier is still contained within the material. The important thing is that in either cases an electric potential is produced by the separation of charges. The core of the photovoltaic energy is precisely the exploitation of this voltage.

4.3.2. Solar Cells

A solar cell is the electrical device that converts the energy of light directly into electricity by the effect mentioned above. In order to properly understand how it works we need to go back to the basics.

4.3.2.1. Semiconductors and Junctions

We are not going to extend ourselves much in this section since it is not the objective of this thesis, nonetheless, having a review may be helpful in order to better understand the principle of operation of a solar cell.

A semiconductor is an element or compound which behaves as a conductor or an insulator depending on various factors such as temperature or illumination. This behavior has to do with the structure as the breakage and formation of bonds are responsible of pair electron-hole formation. Holes, or the absence of an electron, are of utmost importance as the concentration of these together with electrons define the nature of the semiconductor. The existence of these electron-hole pairs is possible thanks to the

characteristic band structure of semiconductors, with a full valence band and an empty conduction band at 0K. An increase in temperature gives some electrons enough thermal energy to jump to the conduction band. Electrons can also gain energy and jump to the conduction band (CB) by absorbing a photon with an energy equal or higher than the energy gap (E_g) between bands (bandgap).Electrons in the conduction band and holes in the valence band (VB) are known as charge carriers and are responsible of conductivity. In order to take advantage of this effect the charges must be separated and extracted; therefore, a **PN-Junction** is needed.

Adding different elements known as dopants to the structure may increase or decrease the concentration of charge carriers. An **intrinsic** semiconductor has the same concentration of holes (p) and electrons (n) ($p = n = n_i$), but modifying these concentrations leads us to **p-type** semiconductors, where $p > n = n_i$, and **n-type** semiconductors, where $n > p = n_i$. In a p-type, holes act as the majority carriers while electrons are the minority carriers. In an n-type the opposite is true. Taking both semiconductors and placing them togethers gives place to the **PN junction.**

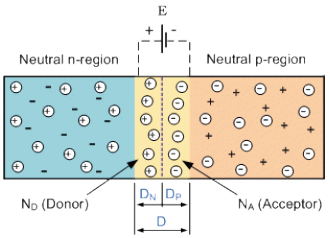

Figure 4: PN Junction. [11]

In **Figure 4** we can see the basics of a PN Junction. The left side corresponds to the N-region whilst the right side is the P-region. When the two semiconductors are in contact two phenomena occur. Due to the gradient of charge carriers, holes from the N-region tend to diffuse to the P-region and the same thing happens to electrons from N-side. As the ions forming the crystal lattice can't move, the diffusion of charge carriers leads to the formation of a voltage, and the consequent electric field. The zone containing the electric field is known as **depletion zone** or **space-charge region (SCR)** as it is almost empty of charge carriers. This electric field tends to take back electrons and holes, this phenomenon is known as drift. When both forces, drift and diffusion, are equal it is said

that the PN Junction is in an equilibrium state. One more thing we should know before explaining how the solar cell operates is what happens to the junction when a bias is applied. We can distinguish forward bias from reverse bias. The former refers to the situation when an external voltage is applied across the solar cell such that the electric field formed by the junction is decreased. In this situation, due to the external field applied, the existing equilibrium in the junction is disturbed causing an increase on the diffusion current. The increased diffusion causes minority carrier injection at the edge of the depletion region and these carriers will continue diffusing until recombination. The majority carriers needed are supplied from the external circuit and hence a net current flow under forward bias. As recombination is needed for this current to flow, we can say it is a recombination current. The higher the rate of recombination, the greater the current which flows across the junction. In fact, a very important parameter known as "**dark saturation current**" (I_0) is a measure of recombination in a device.

The other situation we mentioned is the reverse bias. In this case a voltage is applied across the device such that the electric field at the junction increases. This increase on the electric field lowers the probability that carries diffuse from one side to the other.

4.3.3. Fundamentals of Solar Cell Operation

As we can see in **Figure 5** the basic structure of a solar cell is no other thing than a PN-Junction. Normally the larger side is called **base** or **absorber** while the smaller side and the closest to the sunlight is called **emitter**. Other important parts are the front and back contact, but we will talk about them later.

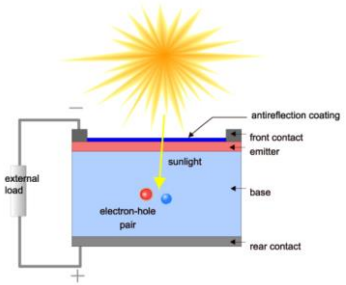

Figure 5: Cross section of a solar cell. [11]

The basic steps in the operation of a solar cell can be summarized in: the generation of light-generated carriers; the collection of the light-generated carriers to generate a current; the generation of a large voltage across the solar cell and the dissipation of power in the load and in parasitic resistances. Now let's analyze with more detail these basic steps.

4.3.3.1. Light Generated Current and Collection Probability

The incident photons from sunlight are absorbed thus causing the creation of electron-hole pairs. For this to happen the photon's energy must be higher than the band gap. An important thing to consider is that these carriers have an average lifetime, which means that sooner or later they will recombine. It is important trying to avoid recombination as this would result in the loss of the electron-hole pair and no current would be generated. In order to avoid recombination, the needed process after generation is the collection. This process consists in separating the carriers by means of the electric field generated between emitter and base. If these two are connected, the light generated current will flow through the external circuit. Both generation and collection determine the light generated current from the solar cell.

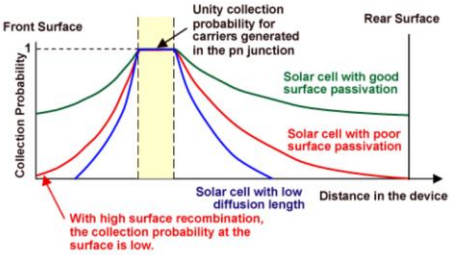

Figure 6: Different collection probability scenarios in a solar cell. [11]

4.3.3.2. Quantum Efficiency and Spectral Response

The quantum efficiency is the ratio of the number of carriers collected by the solar cell to the number of photons of a given energy incident on the solar cell. Ideally, the QE should be close to one for all the spectrum but due to recombination effects, optical losses and low photon absorption this efficiency tends to be reduced. We can differentiate "external" QE from "internal" QE. The former includes the effect of optical losses such as transmission and reflection while the second only refers to those photons that are neither

transmitted nor reflected. Measuring the reflection and transmission of a device is useful in order to correct the external QE and obtain the internal QE curve.

Similarly to QE, spectral response is the ratio of the current generated by the solar cell to the power incident on the solar cell. Both QE and spectral response are used in solar cell analysis and the choice depends on the application.

4.3.4. Solar Cell Parameters

In this section we are going to see the most important parameters that should be considered in a solar cell. But first of all, it is important mentioning the IV curve. This curve is the superposition of the IV curve of the solar cell diode in the dark with the light-generated current. When the solar cell is under light conditions the resulting IV curve is down shifted to the fourth quadrant where power can be extracted. In this condition the diode law becomes:

$$\boldsymbol{I = I_0\left[\exp\left(\frac{qV}{nkT}\right) - 1\right] - I_L} \qquad \text{Equation 1}$$

Where I_L is light generated current, kT is the product of the Boltzmann constant and the temperature, q is the elementary charge, V is the potential and I_0 the dark saturation current.

Plotting the above equation gives the IV curve. Many important points are contained within this curve as we can see in **Figure 7**. It is important noticing that the curve has been reversed for practical reasons, it is easier working in the first quadrant than in the fourth.

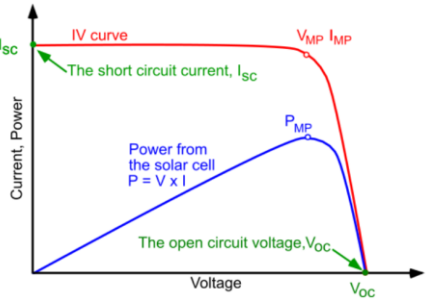

Figure 7: Illuminated current-Voltage curve of a solar cell. [11]

4.3.4.1. Short-Circuit Current (I_{sc})

Short circuit current is simply the device current when V = 0. Imagine a situation where charges can freely escape the solar cell thorough a non-resistive wire. At some point equilibrium will be reached and, after that, all charges generated that do not recombine will flow to through the external circuit thus generating current. In the ideal case, I_{sc} is equal to I_L. Since the charges can flow freely through the wire and recombine, no voltage can build up and no power can be extracted from de cell.

4.3.4.2. Open-Circuit Voltage (V_{oc})

The opposite situation is when charges cannot escape the solar cell. This voltage is the maximum that a solar cell can deliver. It corresponds to the forward bias voltage, at which the dark current density compensates the photocurrent density. The open-circuit voltage (V_{OC}) depends on the saturation current density of the solar cell and the photocurrent density but the key effect is the saturation current. Since this current depends on the recombination, V_{OC} it is also a measure of the amount of recombination in the device.

4.3.4.3. Fill Factor (FF)

The fill factor is the ratio between the maximum power ($P_{max} = I_{MP} \cdot V_{MP}$) generated by a solar cell and the product of V_{OC} and I_{SC}.

$$\boldsymbol{FF} = \frac{\boldsymbol{I_{MP}V_{MP}}}{\boldsymbol{I_{SC}V_{SC}}} \qquad \text{Equation 2}$$

It is also a measure of the squareness of the IV Curve. The highest the FF, the closest to an ideal device.

4.3.4.4. Efficiency

The last parameter we are describing is the conversion efficiency. This is the ratio between the maximal generated power and the incident power. Typically, all these parameters are measured under standardized conditions. Those conditions, known as

STC where the incident light is described by the AM1.5 spectrum, have an irradiance of I_{in} = 1000 W/m^2.

$$\eta = \frac{P_{max}}{I_{in}} = \frac{I_{MP}V_{MP}}{I_{in}} = \frac{I_{SC}V_{OC}FF}{I_{in}} \quad \text{Equation 3}$$

In order to have a complete view of the solar cell we still have to talk about something we have been ignoring until now. Unfortunately, solar cells are not ideal diodes, they present resistance. These can be encompassed in two terms: the series resistance (R_S) and the shunt resistance (R_{sh}). The former includes all the resistive losses along the device while the latter accounts for losses caused by alternative current paths. The final equation to describe the solar cell would be:

$$I(V) = I_0\left[\exp\left(\frac{qV-qIR_s}{k_BT}\right)-1\right]+\frac{V-IR_s}{R_{sh}}-I_L \quad \text{Equation 4}$$

This equation describes the circuit shown in **Figure 8**. However, this equation works well form ideal p-n homojunction solar cells. But in the case of far from ideal p-n junctions, such us heterojunctions, important losses due to recombination in the SCR must be taken into consideration. This is done by adding a quality factor, A, to the Equation 4:

$$I(V) = I_0\left[\exp\left(\frac{qV-qIR_s}{Ak_BT}\right)-1\right]+\frac{V-IR_s}{R_{sh}}-I_L \quad \text{Equation 5}$$

This factor varies from 1 (ideal solar cell with mainly radiative recombination at the neutral region) to 2 (main recombination at SCR).

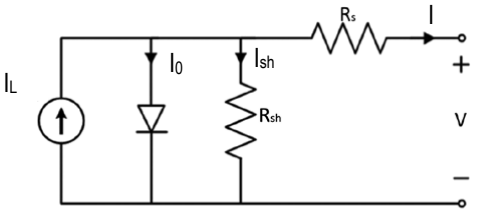

Figure 8: Equivalent circuit of a solar cell with resistive and shunt losses. [12]

4.4. AVAILABLE TECHNOLOGIES

The history of the evolution of photovoltaic technologies can be divided in three generations. The first generation corresponds to crystalline silicon based solar cells, that are the most extensively studied and used nowadays [13]. We can differentiate mono-crystalline from poly-crystalline. The second generation introduced thin film technologies promising lower production costs by reducing both material and energy consumption during manufacturing. The most important technologies in this generation are CIGS and CdTe which will be reviewed later. Finally, the third generation arrived proposing new thin film alternatives such as Perovskites, Zinc Phosphide and Kesterites.

4.4.1. Crystalline Si Solar Cells

With around a 90% of market share crystalline Si-based cells are the dominant PV technologies [14]. This technology is based in p-n homojunctions of silicon doped with boron for the p-side and phosphorus in the n-side. As said before we can distinguish monocrystalline cells (c-Si) and polycrystalline cells (p-Si).

Monocrystalline cells rely on very high purity monocrystalline Si wafers. Very high efficiencies are achieved thanks to the lack of defects and grain boundaries. Although it has been already said that Si-based solar cells are p-n homojunctions, the truth is that heterojunction concepts have also been successfully developed. In fact, this technology holds the record with a 26.7% efficiency. The average commercial c-Si solar panels have efficiencies around 15-19% with the best ones surpassing 20% [15]. The problems with this technology are the high energy consumption, the price and the complicated process required to obtain them. In order to reduce costs, p-Si technology appeared from obtaining polycrystalline ingots from molten Si. Controlling temperature during the cooling is important in order to obtain a columnar structure.

The higher concentration of defects due to dangling bonds at the grain boundaries plus dislocations and point defects lowers the efficiency. Despite this, a record efficiency of 22.6% has been achieved thanks to extensive research in crystal growth and defect passivation [16]. Commercial panels currently range 13 to 17% efficiency with a 50% of market share.

These efficiencies may seem low but achieving them with other technologies is a big challenge. The question that arises is, why do we need new technologies? Due to several reasons the fabrication of c-Si and even p-Si is very expensive:

i. Si is the second most abundant element in the earth crust but in the form of SiO_2. In order to reduce it to metallurgic-grade Si (98% purity) very high temperatures (~1800ºC) are needed. This process requires around 50MJ to produce 1 kg of Si.

ii. Metallurgic-grade Si must be purified via high temperature (~1300ºC) chemical vapour deposition (CVD). This is because of the covalent nature of Si-Si bonds, in combination with an indirect 1.14 eV gap, results in a poor defect tolerance.

iii. The manufacturing of Si ingots requires melting the purified metal again as well as a complex pulling/casting process.

iv. Due to the low light absorption and fragility of Si, wafers with thicknesses >100 µm are required. During the sawing process a considerable amount of material is lost so that 3-9 g of raw Si (before sawing) are necessary per peak watt (Wp) at the module level.

To sum up, even though the price of Si has fallen in the last years the embedded energy of this technology barely compensates its good performance. This statement can be verified by calculating the energy returned on investment (EROI) where it gets low values compared to other PV technologies (**Figure 9**). It has been demonstrated that changing the Si wafers obtention process with the intention of reducing energy consumption is extremely challenging thus it is better developing new technologies.

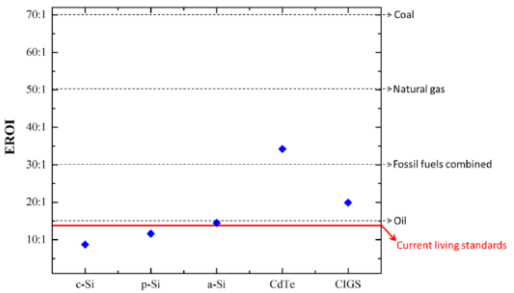

Figure 9: EROI of the main PV technologies compared to fossil fuels. [12]

4.4.2. Thin Film Technologies (CIGS-CdTe)

4.4.2.1. Amorphous Silicon

Before the emergence of these two technologies (CIGS and CdTe) the first thin film solar cell to be commercialized was based on amorphous Si. The addition of hydrogen to the structure improved the quality of the material by passivating the dangling bonds occurring naturally due to its amorphous structure. This new material has a 1.7 eV bandgap and a very high absorption coefficient (~10^5 cm^{-1}) that allows reducing the absorber layer below 1 μm resulting in a solar cell with a total thickness of ~2 μm. Unfortunately, the presence of hydrogen causes a light-induced degradation known as the Staebler-Wronski effect which causes an increase in defect density that implies an increase in the recombination current thus reducing the efficiency of the cell. In addition to this problem, commercial modules only present an efficiency around 7%.

4.4.2.2. CdTe

Cadmium Telluride is an II-VI compound with a bandgap of 1.45 eV which corresponds well to the sunlight spectra [17]. It has a large absorption coefficient due to its direct transition allowing the use of thin films. Its usability was first demonstrated in 1963 by a General Electric Research Laboratory [18] but it wasn't until 1972 that the p-CdTe/n-CdS was presented with a moderated efficiency of 6% but also showing a better stability. Soon after it was discovered that a superstrate configuration led to more efficient devices. Its favorable properties and the continuous development of the technology have converted CdTe in a mature PV technology with a record efficiency of 22.1% and commercial modules ranging 15-18% competing directly with Si with a 3% market share.

Moreover, First Solar claims that CdTe has the lowest energy production cost which, according to them, makes this technology the most ecofriendly technology available. However, the toxicity of Cd and the scarcity of Te may limit the future production [12].

4.4.2.3. CIGS

This technology is especially important since it is the technology on which the kesterite is based. The first appearances of CIS ($CuInSe_2$) as a potential PV candidate took place in 1976, when the first thin film was fabricated with an efficiency around 5%. CIS is a ternary I-III-VI_2 chalcogenide semiconductor with a chalcopyrite crystal structure, naturally

occurring p-doping and a high absorption coefficient (>10^5 cm^{-1}). It has a direct bandgap of 1.04 eV but a great discovery was made when researchers found out that substituting In atoms by Ga atoms widened the bandgap thus improving its overall properties. This way, by modifying the proportions of $CuInSe_2$ and $CuGaSe_2$ we get $Cu(In,Ga)Se_2$ and the possibility of tuning the bandgap of the material from 1 to 1.7 eV. Furthermore, the substitution of Se by S atoms allows even more bandgap tuning. As in the case of CdTe, CIGS devices are based on the heterojunction with CdS. The fabrication is carried out in substrate configuration employing typically soda-lime glass (SLG). A Mo contact is deposited onto the glass followed by the CIGS absorber and the CdS/TCO window layer. TCO stands for Transparent conducting oxide and acts as a front contact. The deposition of CIGS can be achieved both by physical and chemical ways although physical routes usually result in better performances. The common physical procedure consists of depositing the metallic precursor by means of a sputtering followed by a reactive annealing in S/Se atmosphere. Another commonly employed procedure consists of the co-evaporation of Cu, In, Ga and S/Se.

Nowadays it is the thin film commercial technology with the highest reported efficiency 23.35%. Commercial modules range 14-17% with the most advanced ones, by Solar Frontier, exceeding 18%. Its market share is around 2%. Since it is a quaternary compound the compositional precision required during the fabrication process makes it a more expensive technique than CdTe. Finally, the fact that both In and Ga are rather scarce poses a problem. The solution one could think is, what if we use earth abundant materials to build devices? That is precisely the intention of kesterites.

4.5. EMERGING THIN FILM TECHNOLOGIES

As we have seen, all available technologies have some problem whether it is production costs, the usage of toxic or scarce materials, or the fact that they are too rigid prevents certain potential applications. Some of the emerging technologies aim to solve these problems. Let's review some of the most promising ones without going into tandem or multi-junction technologies.

4.5.1. Perovskites

Perovskite solar cells (PSC) are based in perovskite structured compounds. These ternary compounds can be oxides, nitrides, halides and others. They are described by an ABX_3 crystal structure where A and B are cations and X is an anion. The most common perovskite absorber is methylammonium (A) lead (B) trihalide (X), where the halogen ion and its content can vary the bandgap from ~1.55 to 2.3 eV [19]. This technology has gained tremendous attention in the PV industry due to its unique characteristics such as good flexibility, low cost, good scalability, low temperature processability and comparable PV performance compared with traditional thin film technologies [20]. One drawback, related to the easy processability via solution, is the vulnerability of the halide perovskites with respect to moisture or polar solvents since these compounds are salts with a noticeable solubility product in many solvents. Other problems related to this technology are the need of using a toxic metal and a very expensive metal. These are lead and cesium respectively. To finish, it is worth mentioning that this material degrades with light. The solution to this problem is an encapsulation that is extremely expensive.

4.5.2. Organic-Based Solar Cells

The two most important benefits of organic photovoltaic devices (OPV) based on organic semiconductors are the cost-effective fabrication processes and the possibility of producing organic semiconductors in flexible substrates [20]. The technology of organics-based PV derives from the principles of dyes and pigments. The active materials are synthesized from petrochemicals and do not contain scarce or toxic elements. Historically this technology has split into two main branches: dye-sensitized and donor/acceptor heterojunction, both with several sub-species. The parallel development helped generating and refining a general picture on the value, potential and challenges of organics-based cells and other thin film PV technologies [14].

4.5.3. Kesterites

The success of CIGS and CdTe stimulated intense research for new chalcogenide absorbers in photovoltaics. Several chalcogenides have been tested and two compounds reached efficiencies above 10%. These are Cu_2S and $Cu_2ZnSn(S,Se)_4$ (CZTS). The

former suffers from stability issues due to the diffusion of copper, but the latter is considered as one of the most promising future absorber materials. It is composed of non-toxic and abundant materials. CZTS is derived from the naturally occurring mineral kesterite. The crystal structure is based on the diamond -like aristo-type structure just like GaAs, CdTe or $CuInS_2$. All these structures can be derived from the diamond structure by substituting the tetravalent atom (i.e., Si) by atom combinations with an average of four valence electrons (**Figure 10**). CZTS is the natural evolution of CIS technology. Substituting the trivalent indium by the bivalent zinc and the tetravalent tin we arrive to the desired structure. It is common to refer to this technology as CZTS, but a more proper way is CZTSSe since by varying the selenium-to-sulfur ratio, the band gap can be tuned from 1.5 eV for the pure sulfide to 1.0 eV for the pure selenide.

As CIGS is the parent technology for this absorber, the same device architecture is used to collect the charge carriers. The n-type counterpart typically consist in a thin CdS layer, but also Zn(S,O,OH) can be employed to avoid toxic Cd. [14]

Despite being able to use the CIGS device architecture, it is no optimized for kesterite, so further research must be done. In addition of improving the architecture, kesterite formation should be thoroughly investigated as several problems prevent these cells from performing to their full potential. The aim of these paper is trying to solve one of these problems, specifically, the problem associated with incorporating tin into the structure. As we will see in the next section, the kesterite formation depends on several factors [21].

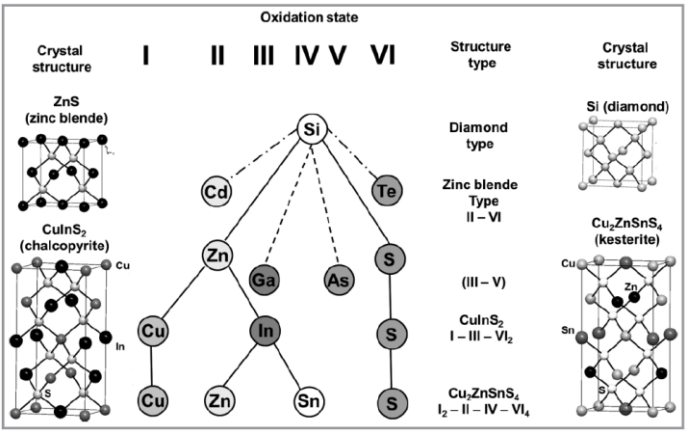

Figure 10: Schematic illustration of the origin of $Cu_2ZnSnSe_4$.

5. KESTERITE STATE OF THE ART

In this chapter different properties of the kesterite will be discussed. In the preceding section we have seen a brief introduction to this promising technology. Now let's explore all that it has to offer starting with its structural properties.

5.1. STRUCTURAL PROPERTIES

5.1.1. Crystal Structure

The compound semiconductors CZTS, CZTSe as well as the solid solution series CZTSe most commonly crystallize in the kesterite-type structure [22]. In this type of structure, one Cu occupies the 2a (0,0,0) position, with Zn and the remaining Cu ordered at 2d (0,1/4,3/4) and 2c (0, 1/2, 1/4) respectively. Sn is located at 2b (0,0,1/2) and anion lies on the 8g (x, y, z) position. A representation can be seen in **Figure 11**.

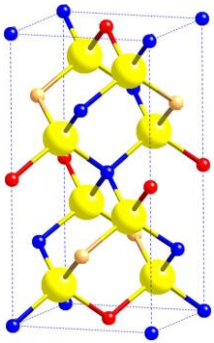

Figure 11: Unit cell representation of the kesterite-type crystal structure. Anions are represented by yellow spheres and cations are represented by the smaller spheres (blue-Cu^{+}, red-Sn^{4+} and orange-Zn^{2+}). [22]

It has already been seen how the structure can be obtained from the diamond itself by substituting atoms respecting the octet rule. The similar structural features between CIGS and CZTSe gives rise to similar optical and electronic properties as it will be shown later. Two principal crystallographic structures have been identified for CZTSe, the

already known kesterite type and the stannite type [23]. However, calculations have shown that the kesterite phase formation is slightly less energetic than the stannite, being more stable [24]. This structural difference can be seen in **Figure 12**. Due to its similarities XRD makes difficult its discrimination thus neutron diffraction may be needed [22]. Another important aspect to take into account is the possible (and probable) presence of secondary phases and in order to discriminate them Raman spectroscopy is used [25]. More about these secondary phases will be discussed further on. In addition to these phases, disorder in the Cu-Zn lattice planes can occur when fast cooling of the synthesized kesterite takes place [22], [26]. This disorder can be reversed with an annealing at a temperature lower than 200ºC (for pure CZTSe) and it is relevant since it was theoretically demonstrated that order has influence on the bandgap [27]. Another interesting characteristic of kesterite based solar cells is that the highest device performance is obtained for a Cu-poor and Zn-rich composition (known as A-type kesterite) with cationic ratios around Cu/(Zn+Sn) = 0.8 and Zn/Sn = 1.2 [28].

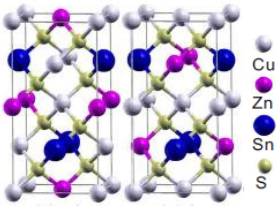

Figure 12: The crystal structure of kesterite (left) and stannite (right). [23]

The reason for the A-Type kesterite better performance can be found in the intrinsic defect structure of the material. Theoretical calculations of Chen et al. show that Cu-poor Zn-rich composition enhances the p-type conductivity due to the increased density of Cu vacancies which act as a main intrinsic swallow acceptor. In addition, A-type kesterite prevents the formation of [$2Cu_{Zn}$ + Sn_{Zn}] defect clusters which has low formation energy in stoichiometric composition. These defects act as electron trapping states in the absorber with its consequent harm in solar cell performance. On the other hand, [V_{Cu}+Zn_{Cu}] and [Zn_{Sn} + $2Zn_{Cu}$] defect clusters are expected in A-Type Kesterite. Fortunately these clusters are electronically benign and do not harm solar cell performance [29]. Apart from what has been mentioned above, other defects are present limiting the efficiency adding non-ideal recombination paths.

As you can see, obtaining the desired structure is not an easy task in a quaternary compound in which so many variables come into play. As far as this work is concerned, the variable that will be emphasized is the incorporation of tin to the structure. Later on, we will see that during the synthesis, the formation of volatile tin secondary phases represents a loss of this element, which in turn entails a loss of performance.

5.2. ELECTRICAL PROPERTIES

Optical and electrical properties are essential to understand and solve the voltage (V_{oc}) deficit in kesterites [26]. Even the CZTSSe solar cells with the best performance suffer from low V_{oc} (never better than 60% $V_{oc\ max}$) [21]. In terms of electrical properties, the four following aspects and its impacts are generally discussed: minority carrier lifetime, charge carrier concentration, charge carrier transport, and the variability of conductivity. The minority carrier lifetime (τ) is a critical parameter because it's a measure of the net recombination rate, which is a direct relation with the V_{oc}, a parameter of particular concern for kesterites [30]. For highly defective materials such as kesterites, complex carrier transport and dynamics as well as high recombination rates make accurate extraction of τ quite challenging. Relatively recent work indicates that τ is in the sub-nanosecond regime for kesterites [31]. Presently, defect recombination in the bulk kesterite material via non-radiative defects is suspected as the culprit for the low lifetime [32]. In order to determine the origin for this rate limiting recombination several analyses are being carried out. A general consensus among many kesterite researchers is that limitations in kesterite performance arise from the bulk absorber rather than from its interfaces [32]. Despite many mechanisms can be responsible for this, some of them such as radiative recombination can be quickly disregarded. On the other hand, both shallow and deep defects are expected to play an important role in explaining the non-radiative losses measured in kesterites. A relative comparison of the various loss mechanism is shown in **Figure 13**.

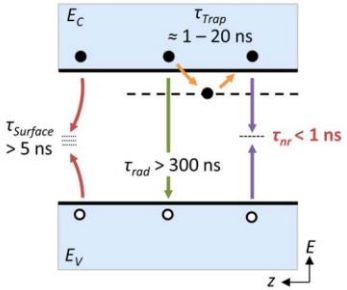

Figure 13: Schematic representation of various recombination mechanisms which contribute to the minority carrier lifetime in kesterite, and their relative impact. τ_{Trap} is the trapping/de-trapping time, $\tau_{surface}$ is the surface recombination lifetime, τ_{rad} is the radiative lifetime in low injection, and τ_{nr} is the non-radiative lifetime. [30]

Another point of interest that continues being discussed nowadays, is the transport of charge carrier's mechanisms. Carrier transport properties including carrier type (p or n), density and mobility are of fundamental importance. The majority carrier density affects recombination lifetime and depletion width, while the carrier mobility, specifically for the minority carriers, affects diffusion length. Carrier density can vary from $1 \cdot 10^{19}$ cm^{-3} for a stoichiometric sample to $1 \cdot 10^{15}$ for the record IBM device with Cu/(Zn+Sn) = 0.85 and S/(S+Se) = 0.25. Best devices typically contain about 20%-30% sulfur and are, again, Cu-poor. The ideal predicted carrier density is below 10^{16} cm^{-3}.

The transport of carriers can take place either by drift in electric fields or by diffusion. Either way, mobility plays a decisive role. Typical values for different technologies range from 1 cm^2 V^{-1} s^{-1} or less, to several thousands of cm^2 V^{-1} s^{-1}. Charge carrier mobilities depend on fundamental material properties such as the effective masses of the conduction band minimum and the valence band maximum, carrier-impurities, etc. In the case of kesterite, values range from about 0.5 cm^2 V^{-1} s^{-1} to more than 100 cm^2 V^{-1} s^{-1} as a function of S/(S+Se) content and Cu/Zn + Sn.

In order to better understand the limiting factor of kesterite solar cells, in **Table 2** a comparative between kesterite and its parent technology (CIGS) is given.

Table 2: Comparison of electrical properties of CIGS and CZTSSe

Absorber	Carrier Density (cm^{-3})	Mobility ($cm^2 V^{-1} s^{-1}$)	Minority carrier lifetime
CZTSSe	10^{15} – 10^{19}	0.5 - 100	<1 ns
CIGS [12], [33]	10^{15} - 10^{17}	5 - 9	~10-100ns

As it can be seen from the table, the biggest difference between these two technologies is the much lower carrier lifetime for kesterites. As for the other properties, they can be easily controlled thus efforts should be focused on minimizing the defects responsible for lifetime loss. In **Figure 14** most the defects are shown. Notice that most of the deep defects are Sn related thus special attention must be paid to Sn dynamics during incorporation.

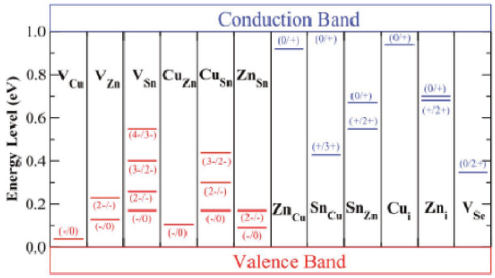

Figure 14: Ionization levels of intrinsic defects in the bandgaps of CIGSSe. The red bars show the acceptor levels and the blue bars show the donor levels, with the initial and final charge states labeled in parenthesis. [21]

5.3. Optical Properties

One of the main reasons of interest in kesterite CZTSSe absorber materials for thin film solar cells is due to its high absorption coefficient of ~10^4 cm^{-1}. The expected bandgap is 1.5 eV for CZTS and 1.1 eV for CZTSe [34].

Table 3: Comparison of maximum absorption coefficient and bandgap for different technologies

Absorber	E_g (eV)	Absorption Coefficient (cm^{-1})	REF
Silicon	1.7	~10^5	[12]
CdTe	1.45	>10^4	[12]
CIGS	1.0 – 1.7	>10^5	[12]
Perovskite	1.55 – 2.3	~10^4	[19]
CZTSSe	1.1 – 1.5	>10^4	[12]

As it can be seen in **Table 3** there is not much difference between different technologies. In fact, most of them present the possibility of modifying the bandgap according to the composition. The advantage of being able to control the bandgap is that, depending on the application for which the solar panel is intended it may be more interesting to have a higher voltage at the expense of a lower current, or the opposite. In general, the wider the bandgap, the higher the voltage.

5.4. SYNTHESIS METHODS

Historically, based on the similarities between kesterite and chalcopyrite compounds, the standard device structure adopted for (CIGSSe) was directly extended to CZTSSe, by simply replacing the CIGS absorber layer with a p-type CZTSSe thin film.

Prior to explaining the different routes, a review of the architecture currently used will be given. The base of everything is nothing but a soda-lime glass (SLG), the substrate. This substrate is coated with a sputtered Mo layer acting as a rear metallic contact. The typically used thickness for this layer is around 500 nm to 1 μm. The kesterite absorber is then deposited onto the Mo layer. The fabrication of the absorber consists on the deposition of a precursor layer via a physical or a chemical route, followed by a reactive annealing with an atmosphere containing either S (sulfurization) or Se (selenization). A common result during annealing is the formation of a thin $Mo(S,Se)_2$ layer at the CZTSSe/Mo interface with a thickness of a few nanometers. It has been demonstrated that this intermediate layer is p-doped and helps to improve the ohmic character of the

back contact [35]. After the absorber deposition, chemical treatments can be applied to the surface in order to remove secondary phases and/or prepare the surface for the subsequent PN junction formation. The counterpart of the absorber, commonly known as buffer layer is then deposited by chemical bath deposition. Cadmium sulfide (CdS) is normally used and the thickness of the layer ranges from 50 to 100 nm. Above all the last layer called window layer is finally deposited. The window is formed of intrinsic ZnO (i-ZnO) layer and a transparent conducting oxide (ITO) layer both deposited by sputtering with a thickness of 50 – 100 nm and 200 – 400 nm respectively.

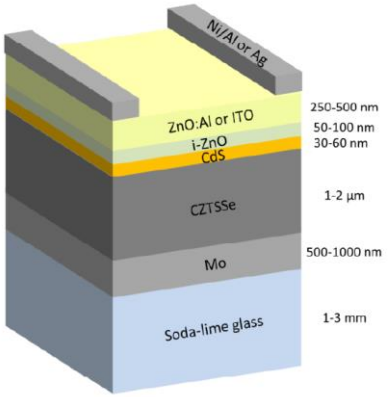

Figure 15: Standard cell configuration and typical layer thicknesses of kesterite solar cells. [12]

In **Figure 15** a completed cell is shown. The objective of this thesis is to improve both precursor layer and reactive annealing conditions. But before going into detail, the different methods currently used will be reviewed.

5.4.1. Physical Routes

Having the general structure of kesterite solar cells in mind, three different types of physical routes used for the synthesis of kesterite thin film as absorber layer are discussed in this section.

5.4.1.1. One-Step Processes

One-step processes are based on co-evaporation of single elements onto pre-heated substrate. The advantage of this method is that in a single step the absorber is synthesized and crystallized. Despite the advantages and the knowledge gained from CIG(S,Se), co-evaporation of CZTSSe has been revealed as very challenging from the beginning [36]. Despite optimizing the co-evaporation parameters in order to get a Cu-poor Zn-rich structure, researchers found that the complexity of the reaction process is due to the subtle reaction obstacle between CuSe and ZnSe species associated to the volatile nature of SnSe phase and/or the physical separation between the binary precursors. In short, the key challenge is to control Sn-volatile species in order to provide an optimized route for the complete formation of the material. Several attempts have been done with the objective of overcoming this problem, but the desired results were not obtained. The next approach requires the inclusion of an additional step at high temperature and under chalcogen and Sn atmosphere, which normally helps to correct possible deviations and improves the growth of crystal grains.

5.4.1.2. Two-Steps Processes

Two-step processes are the most widely used for the growth. These experimental procedures consist of what is set out in the introduction to this section. First a deposition of a precursor of a film containing all (or part of) the chemical elements necessary for the kesterite phase formation, followed by a thermal annealing treatment under S or Se containing atmosphere. Different PVD techniques can be used. The most relevant results obtained by evaporation, sputtering and PLD are presented in the following sections.

5.4.1.2.1. Sequential evaporation/Co-evaporation

In order to minimize the risk of secondary phases formation during the growth process, thin films can be deposited by co-evaporation or sequential evaporation at low temperatures followed by reactive annealing at high temperatures. It was demonstrated

that an annealing step at high temperature under Sn-containing atmosphere is highly necessary to compensate the Sn loss [37]. The highest CZTSe-based cell efficiency obtained by this method is 11.6%, very close to the current record [38].

In comparison to chemical processes, the synthesis of kesterite absorber layers using co-evaporation provides a better reproducibility, higher material quality and safer methods to work with Se and/or S compounds.

5.4.1.2.2. Sequential sputtering/Co-sputtering

Sputtering-based techniques have proved to be an efficient physical route for the synthesis of high efficiency thin film devices. CZT(S,Se) can be classified depending on the targets used and on the deposition sequence. As for the targets, both pure metallic (Cu, Zn, Sn) and metallic alloys (Cu-Sn, Zn-Sn) have been used as well as chalcogen-containing targets. Concerning the deposition sequence either stacked layer (sequential sputtering) and homogeneously mixed (co-sputtering) precursors have been studied.

One of the advantages of sequential sputtering is the possibility of modifying the stack structure and optimize the reaction pathway for kesterite formation. Moreover, by simply tuning the thicknesses and the stacked layers, control of composition is easier than the co-sputtered route. It is worth emphasizing, that the current efficiency obtained by sputtering methods is well above 10% [36].

The discovery that using a mixed a Cu-Sn target reduces the Sn loss by driving the system towards the formation of related ternary compounds Cu_2SnX_3 (with X = S or Se), rather than binary volatile SnX phases is of great importance for this thesis, since the experimental will deal will this issue. It was shown that an annealing pressure around 10 mbar allows the minimization of loss volatile species. The latest developments of the process include a growth of Cu-poor CZTSe via **an intermediate Cu-rich state**, which appears to stabilize the reaction path and allows for more defined control of the final material properties.

The following stack is currently used at IREC. The precursor is deposited on a specifically designed Mo tri-layer (a first layer to improve back contact adhesion and conductivity, a more porous middle layer that practically doesn't form $MoSe_2$, and a sacrificial final layer that will form $MoSe_2$ with a controlled thickness). The typical precursor

structure consists of Zn (165 nm) / Cu (175 nm) / Sn (275 nm) / Cu (5 nm) / Mo. This configuration allows to obtain a Cu-poor (Cu / (Zn+Sn) = 0.72) and Zn-rich (Zn/Sn = 1.05) structure [35]. The 5 nm thick Cu layer is deposited in order to improve Sn wettability onto the Mo substrate. Then the 275 nm Sn layer is deposited at the back of the absorber layer to delay and avoid evaporation of Sn(S,Se) phases as much as possible. Subsequently a 175 nm Cu layer is grown facilitating the formation of bronzes (Sn-Cu alloys) and brasses (Zn-Cu alloys) stabilizing both Zn and Sn. Finally, a 165 nm thick Zn layer is deposited in excess at the top of the absorber layer in order to keep the excess at the surface for further removal. Afterwards the metallic stack is submitted to a reactive annealing under Se and Sn atmosphere using a graphite box in a tubular furnace, with a first annealing at 400ºC for synthesizing the kesterite and a second step at 550ºC for its improved crystallization.

About co-sputtering, it is worth knowing that the most widely and successfully used processes are based on binary compound or mixed metallic compound targets, sputtered in an inert atmosphere. The main difference between these two approaches is the chalcogen amount in the starting precursor.

5.4.1.2.3. Pulsed Laser Deposition (PLD)

This technique has been used for a relatively short period of time and the efficiencies obtained are not close to those obtained by the other methods already seen. The method typically consists in strucking a CZTS or Cu_2ZnSnO_4 target with a KrF excimer beam. After the deposition, the films are annealed in a graphite box with a S overpressure at a temperature ranging from 550ºC to 600ºC. It has been observed that the stoichiometry of the deposited film is strongly dependent of the laser energy per unit area [$J \cdot cm^{-2}$]. For the desired stoichiometry with a Cu-poor Zn-rich film, a fluence in the range of 0.7 - 1 $J \cdot cm^{-2}$ must be used. The record efficiency obtained reached 5.4% [39].

Despite attempts to improve efficiencies, several issues significantly hurdle the production of high-efficiency solar cells based on absorber layer grown by PLD [40], [41]. Moreover, laser equipment is expensive, and this may be the biggest obstacle for a wide-spread use of PLD in PVs.

To sum up, we have seen that physical procedures used for the synthesis of the absorber layer has demonstrated the capacity of producing devices with comparable efficiencies than those reported by chemical routes. The better control of grain growth, the limitation of both Sn(Se,S) losses during annealing and secondary phases has helped to minimize the Voc deficit, although there is still a lot of room for improvement. The optimized sequential sputtering route has proven to be probably the best alternative today or at least the most promising one.

5.4.2. Solution-Based Synthesis

Solution based methods is the other possibility available. Since it is not the route used in this work, the review will be purely informational. Since investigations into the use of CZTSSe for photovoltaics began in 1988 over 2900 papers have been published. Of these publications, over 65% have investigated liquid processed layers. These layers contained all the necessary elements to form the kesterite in a subsequent annealing. There are several different possible solution-based syntheses of kesterite layers. Here we will see very briefly what they are, as well as some of their advantages and disadvantages. The first advantage common to all methods is the possibility of depositing layers uniformly at high speed, with nearly 100% material utilization, using low-capital equipment. To do so, solutions or 'inks' containing the elements (and some others) are used. Consequently, the main challenge lies in removing all the other components of the solution from the precursor film since most semiconductors are very sensitive to impurities.

5.4.2.1. Synthesis Methods

The first method capable of providing precise, homogeneous target composition and facile crystallization of the desired phase, minimizing secondary phase formation and providing device-quality interfaces were **hydrazine-based suspensions and solutions**. In addition to address all these challenges, this method enabled to surpass the 10% PCE milestone. This solvent presents unique properties for research on multinary chalcogenide materials, such as the absence of carbon and oxygen or its strong reductive properties that allow the formation of soluble chalcogenide complexes with many metals. These advantages are responsible of producing highly pure crystalline layers with precise composition control. The world record efficiency of 12.6% was achieved by means of this

method [42]. Thanks to the boost in performance many research centers increased their efforts to further improve this technology. Despite all the advantages, the high flammability and toxicity encouraged the development of other solvents capable of achieving equally high efficiencies.

Thus, **aprotic molecular inks** and protic solvents were introduced. The advantage of aprotic solvents is that they lack a reactive oxygen site, thus avoiding the formation of metal-oxygen-metal bonds or metal-oxygen-carbon bonds, which can be difficult to eliminate. A widely studied molecular ink route studied is based on DMSO (di-methyl-sulfoxide) and a sulfur containing complexation TU (thiourea) [43]. The desired oxidation state for cations CZT(S,Se) (+1,+2 and +4 for Cu, Zn and Sn, respectively) may be achieved in the molecular ink by dissolving salts where metals are already in that oxidation state, or in other oxidation states, provided that they have a facile pathway for redox to reach the desired state. The main challenge of this method, which was not so relevant in the hydrazine case, is the elimination of impurities. Primarily carbon, nitrogen and chloride compounds. Despite difficulties, efficiencies greater than 10% have been achieved in several research groups [44].

The third method used combines **protic solvents** (like water and alcohols) and the **sol-gel method**. This method provides a facile and promising route towards low-cost mass production, which allows for precise control over the microstructure and the composition of the layer. The procedure is quite similar to the previous one. The chosen salts must completely dissolve and be stable for hours in order to avoid compositional changes or second phases. Once the suspension or solution is prepared, the next step is coating a Mo coated substrate.

5.4.2.2. Coating Methods

The research-scale methods most used for depositing the absorber layer are spin coating and spray coating. Spin coating involves the application of the liquid to the substrate, followed by an acceleration up to a certain angular velocity rotational speed [45]. The angular velocity results in the ejection of most of the applied liquid where only a thin film is left. The thickness, morphology and surface topography of the obtained film for a particular material is highly reproducible. On the other hand, only a range of thicknesses can be obtained.

The other technique, spray coating, consists in forcing the solvent/ink through a nozzle whereby a fine aerosol is formed. This method is compatible with low viscosity inks and it is suitable for large area deposition. Alcohol-based protic solvents have been the most commonly explored for spray coating since it allows uniform films and fast solvent evaporation [45]. However, the highest efficiencies CZTSSe devices were made by spray-coating employed DMSO as a solvent [44]. The complexity of this deposition process is the reason that the deposition parameters have not yet been optimized. Another drawback of this method is the relatively small grain size and high surface roughness, in comparison to other techniques. Compared to other techniques such as spin coating or dip coating it offers a less material loss, higher sample throughput, and deposition over larger areas.

5.5. PROPOSED MECHANISMS FOR KESTERITE FORMATION

It has already been told that sequential processes based on sputtering followed by reactive annealing provide excellent results. It's true that this complex synthesis process strongly depends on the precursor stacks, but also on the chalcogen atmosphere during the reactive annealing. Considering this, it is concluded that understanding the intermediate phases and possible formation routes for these techniques is essential for their further progress.

It has been demonstrated that reaction pathways for kesterite formation depends on chalcogen availability in the atmosphere during reactive annealing. Considering the case of a selenization reaction, for medium-low chalcogen availabilities the kinetic of the reaction is mainly controlled by the reaction of Cu-Se (CZTSe), Zn-Se and ZnSe binary phases. By increasing the chalcogen availability towards medium-high values, the pathway becomes simpler involving the ternary Cu-Sn-Se compounds reacting with ZnSe [46]. As for the chalcogen availability we define as low [Se] < $1 \cdot 10^{-3}$ g/cm^3, medium $1 \cdot 10^{-3} \leq$ [Se] $\leq 1 \cdot 10^{-2}$ g/cm^3 and high [Se] > $1 \cdot 10^{-2}$ [46]. In order to study the selenization reaction (extendable to sulfurization) we define a generic reaction represented as follows:.

$$\boldsymbol{mM_{(s)} + nSe_{2(g)} \leftrightarrow^{T,t} xCh_{(s)}} \qquad \text{Equation 6}$$

Where M represent all the metals together in the precursor layer and m is their stoichiometric factor in the reaction, Se_2 is the selenium presented in the atmosphere with its correspondent stoichiometric factor n, and Ch represents the formed chalcogen compound. T and t correspond to temperature and time respectively. Selenization is unlike to occur in one single step as Equation 6 states. In order to prove it, several experiments were carried out modifying reaction conditions [46]. With the results obtained plus the data in **Table 4**, two possible pathways can be deduced.

Table 4: Secondary phases observed in CZTSe kesterite compounds. [47]

Secondary Phase	Raman Shift (cm^{-1})	λ_{exc} (nm)
ZnSe	250	442
Cu_2SnSe_3	180	785
Cu_xSe	260	532
$SnSe_2$	314	785
SnSe	151,130	785
$MoSe_2$	240	532

The possible pathway for low chalcogen availability consists in the following reactions:

$$\boldsymbol{Cu_6Sn_{5(s)} + \frac{11}{2}Se_{2(g)} \leftrightarrow^{T=400^{\circ}C,FastRamp} 6CuSe_{(s)} + 5SnSe_{(s)}} \quad \text{Equation 7}$$

$$\boldsymbol{Cu_5Zn_{8(s)} + \frac{13}{2}Se_{2(g)} \leftrightarrow^{T=400^{\circ}C} 5CuSe_{(s)} + 8ZnSe_{(s)}} \quad \text{Equation 8}$$

$$\boldsymbol{Cu_3Sn_{(s)} + 2Se_{2(g)} \leftrightarrow^{T=400^{\circ}C,SlowRamp} 3CuSe_{(s)} + SnSe_{(s)}} \quad \text{Equation 9}$$

$$\boldsymbol{2CuSe_{(s)} + SnSe_{(s)} + ZnSe_{(s)} \leftrightarrow^{T=400^{\circ}C} Cu_2ZnSnSe_{4(s)}} \quad \text{Equation 10}$$

For high chalcogen availability the possible pathway is as it follows:

$$\boldsymbol{Cu_6Sn_{5(s)} + \frac{11}{2}Se_{2(g)} \leftrightarrow^{T=400^{\circ}C,FastRamp} 3Cu_2SnSe_{3(s)} + 2SnSe_{(s)}} \quad \text{Equation 11}$$

$$\boldsymbol{Cu_3Sn_{(s)} + 2Se_{2(g)} \leftrightarrow^{T=400^{\circ}C,SlowRamp} CuSe_{(s)} + Cu_2SnSe_{3(s)}} \quad \text{Equation 12}$$

$$\boldsymbol{Cu_2SnSe_{3(s)} + ZnSe_{(s)} \leftrightarrow^{T=400^{\circ}C} Cu_2ZnSnSe_{4(s)}} \quad \text{Equation 13}$$

Comparing both pathways, it is concluded that the second pathway is preferred. Under high chalcogen availability the kesterite formation is via the reaction between a ternary and a binary compound, which is a simpler route than just binary compounds. The clear advantage is the reduction of unreacted secondary phases after the selenization is completed. Nevertheless, and despite the high chalcogen availability, the binaries route is still observed, although at a much lower extent.

6. EXPERIMENTAL

The main idea of this thesis is to explore the dynamic of Sn during CZTSe synthesis. We have seen that at the time of producing the precursor it is possible to choose between several strategies. One could deposit each metal necessary layer by layer or directly deposit alloys containing the metals of interest. In this project the novelty is to use a bronze that has not been tested before. Until this moment, as we can see in Equation 7 and Equation 10, Cu_3Sn_5 has been used. One of the products found when this bronze reacts with Se is SnSe, the volatile phase which causes a V_{oc} deficit among other things. On this occasion it is intended to form the precursor from the unusual bronze Cu_3Sn (Cu-rich), hoping that the reaction that gives place to the ternary compound will be the main, thus minimizing SnSe formation and consequently avoiding to some extent the loss of tin. Furthermore, different concentrations of tin in the annealing atmosphere will be tested in order to check the effect in the final composition. It is believed that a greater partial pressure of tin will prevent it from leaving the structure to some extent and even some of this tin may be introduced. The protocol followed is the standard in IREC. Before starting depositing metals, the soda lime glasses (SLG) were conditioned via a mechanical cleaning with special soap and subjected to a 50ºC ultrasonic bath cleaning process with the following solvents sequence: acetone, isopropanol and deionized water during 10 minutes for each of them.

6.1. METAL SPUTTERING

Immediately after the substrate was properly cleaned, the Mo back contact layers (~800 nm, 0.3 Ω/□.) were deposited by pulsed DC-magnetron Sputtering (Alliance Concept CT100). The metallic precursors were then sequentially deposited by DC-magnetron sputtering (Alliance Concept Ac-450) following the stack that follows: **Cu_3Sn** (~290 nm) / Zn (~170 nm) or Cu_3Sn (~221 nm) / Zn (~129 nm). This change in the thicknesses is due to the fact that first samples turned out to be thicker than desired after

selenization. Cu-rich Sn-poor compositions was used because this way crystallization is favored, and Sn loss is partially avoided. The transition to a Cu-poor composition will be further discussed.

6.2. REACTIVE THERMAL TREATMENT

In order to synthesize the kesterite phase the precursors were submitted to a thermal annealing. They were first placed inside a graphite box together with crucibles containing Se powder (99,999%) and Sn wire (99.998%) as an additional Sn source. Then, the graphite boxes were introduced into a 3-zone tubular furnace where a 1-step or a 2-step thermal annealing was performed. Several attempts were done modifying the annealing conditions. First samples were annealed in a 1-step process a temperature of 550ºC, an initial pressure of 450 mbar and a final pressure of 845 mbar during 30 min.

Then an almost equal experiment was carried out but modifying the pressures to a final pressure of 10 mbar. Finally, a 2-step process under low pressure conditions was carried out. A first step of 20 mins at 400ºC and 1.5 mbar was followed by a second step of 15 min at the final temperature of 550ºC and 10 mbar.

In all cases samples were naturally cooled down to room temperature. Also, it is worth mentioning that temperature ramps were always 15ºC/min. The result can be seen in **Figure 16**.

The key factor of this treatment was the different quantities of Sn inside graphite box which varied from 50 mg to 500 mg. A constant quantity of 200mg of Se was used.

Figure 16: Kesterite just after being synthesized inside the graphite box. The residue surrounding it is the not consumed Sn.

6.3. MATERIAL CHARACTERIZATION TECHNIQUES

During the fabrication of the devices it is of utmost importance to characterize all the samples. This is important for many reasons. First, to know if the processes are being performed correctly, for instance, checking the composition. But it is also useful as you have different indicators that can allow you to understand the difference between devices yielding different performances. The intention for this work was to use the four techniques mentioned in the title of the section. A brief explanation of its fundamental and why it useful is given below.

6.3.1. X-Ray Fluorescence (XRF)

Each element emits characteristic x-rays when its electrons fall into a lower energy level after being exited upon x-ray illumination. This phenomenon, known as x-ray fluorescence (XRF), is a rapid way to obtain information about the elemental composition of a sample. A Fischerscope XVD XRF analyzer was employed to measure and control **thickness** and **composition** of Mo back contact layers, precursor metallic stacks and kesterite absorbers. The software of this XRF allows creating complex layer models and fits the obtained spectra to them through an iterative process in order to provide the required information of each layer.

6.3.2. Raman Spectroscopy

Raman spectroscopy is an advanced characterization technique based on the analysis of inelastic scattering processes of light with phonons in a material. This technique can be used to determine the presence of different phases in a material, their composition crystalline structure and crystalline quality. In this case, the technique was used to determine the presence of secondary phases and the crystalline quality.

6.3.3. X-Ray Diffraction (XRD)

X-ray diffraction is a technique that allows the identification of crystalline phases in a target. It provides information about their orientation, crystallinity and texture. Unfortunately, due to the exceptional circumstances (Covid-19), these measures could not be carried out.

6.3.4. Scanning Electron Microscope (SEM)

An electron microscope uses electrons as the source of illumination. The shorter wavelength of electrons compared to visible photons makes the resolving power far higher than any standard optical microscope. The FESEM (Field Emission Scanning Electron Microscope) that would have been used, a ZEISS Series Auriga, can detect three types of signal: BSE (backscattered electrons), SE (Secondary Electrons) and characteristic X-rays. The BSE provide spatial-compositional information while SE are useful for performing structural and topographical analyses. As for XRF, the characteristic X-rays gives information about the elemental composition.

6.4. PHOTOVOLTAIC DEVICES FABRICATION

6.4.1. Chemical Etching and CdS Buffer Layer Deposition

Retaking the manufacture of the devices, once the absorber is ready a few more layers are necessary. After depositing the buffer layer, the samples were subjected to 3 successive chemical etchings to remove secondary phases from their surface. An oxidizing etching in a $KMnO_4/H_2SO_4$ solution to remove ZnSe [48]. Then, the samples were placed into a $(NH_4)_2S$ solution to remove Se and Sn(S,Se) [49]. Finally, a diluted KCN etching was done to remove Cu_xSe phases.

After cleaning a 40-60 nm CdS buffer layer was deposited onto the absorber by chemical vapor deposition (CBD). $Cd(NO_3)_2$ (0,12M) was employed as the Cd precursor together with thiourea (0,3M) as the sulphur source. The deposition was carried out with a solution pH = 9.5 and at a temperature of 70ºC for 40 minutes [50].

6.4.2. Window Layer/Front Contact Deposition

After the CdS deposition, an i-ZnO (50 nm) / ITO (200 – 300 nm) bilayer was deposited by DC magnetron sputtering. ITO stands for In_2O_3:SnO_2 and is the layer that acts as front contact. The thickness was controlled by XRF.

6.4.3. Solar Cell Scribing and contact

Once all the layers have been properly deposited, individual 3 x 3 mm^2 solar cells (8.7 mm^2 active) were electrically isolated employing a manual microdiamond scriber (OEG MR200) (**Figure 17**). The scribed lines were performed down to the back contact. A small area at the edges was scratched to expose the back contact and some In was welded onto it.

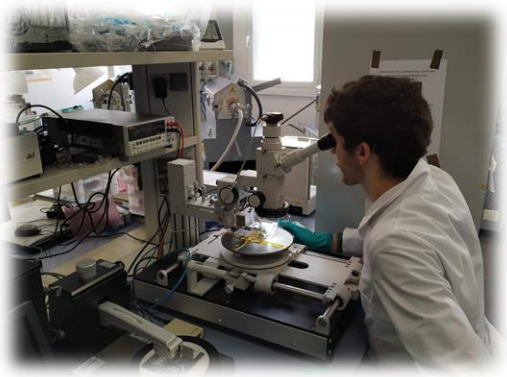

Figure 17: Microdiamond scriber

6.5. PHOTOVOLTAIC DEVICE CHARACTERIZATION

6.5.1. IV-Curve Determination

A setup consisting of a Keithley 2400 source and a pre-calibrated Sun 3000 Class AAA solar simulator by Abet Technologies was employed to carry out the IV measurements of the devices fabricated in this work. The measurements were carried out at 25ºC under simulated AM1.5 illumination (1000 W/m^2). The main parameters of the solar cells were extracted from the curves (V_{oc}, I_{sc}, FF and efficiency).

7. EXPERIMENTAL RESULTS

In **Figure 18** all compositional results obtained by XRF of the kesterites synthesized previously are shown. The samples are split according to the number of annealing steps. As it can be seen, three different cationic ratios are calculated, including: Cu/Zn, Cu/Sn and Cu/(Zn+Sn). The first trend that we can observe is that the Cu/(Sn+Zn) ratio only slightly depends on the Sn availability in the atmosphere, with a tiny increase for the one-step process and a tiny decrease or even no change for the two-steps process.

Focusing on two-steps, it is observed that the higher the Sn quantity in the atmosphere, the higher the Sn concentration into the kesterite structure. This is true until approximately 50 mg of Sn, where the ratio stabilizes no matter the further increase of the quantity of Sn. This suggests that above a certain threshold, the amount of Sn is self-regulated, making the addition of larger amounts unnecessary.

On the other hand, for the one step process the trend seems to be the opposite. We can see that increasing the Sn quantity does not diminish the Cu/Sn ratio as desired or as for the two-steps process. A possible explanation for this behavior is that the process is too fast and high temperatures are reached in a short time, causing the atmosphere not to be able to compensate the Sn loss. This would be justified considering that the more Sn available, the more formation of SnSe compared to $SnSe_2$, being the former more volatile than the latter. This problem does not occur in the two-step process since the first stage at low temperature allows to compensate the loss.

For the Cu/Zn ratios, and as it was expected, no remarkable variations are observed because these two elements do not suffer any exchange with the atmosphere. In summary, Sn is introduced more efficiently from the atmosphere in relatively Sn-poor precursors when two-steps processes are used, thanks to the presence of a lower-temperature step favoring its incorporation. For the one-step process other conditions (P, T, t, m_{Se}, m_{Sn}) needs to be investigated in order to evaluate the potential of this process to introduce Sn from the atmosphere in Sn-poor precursors.

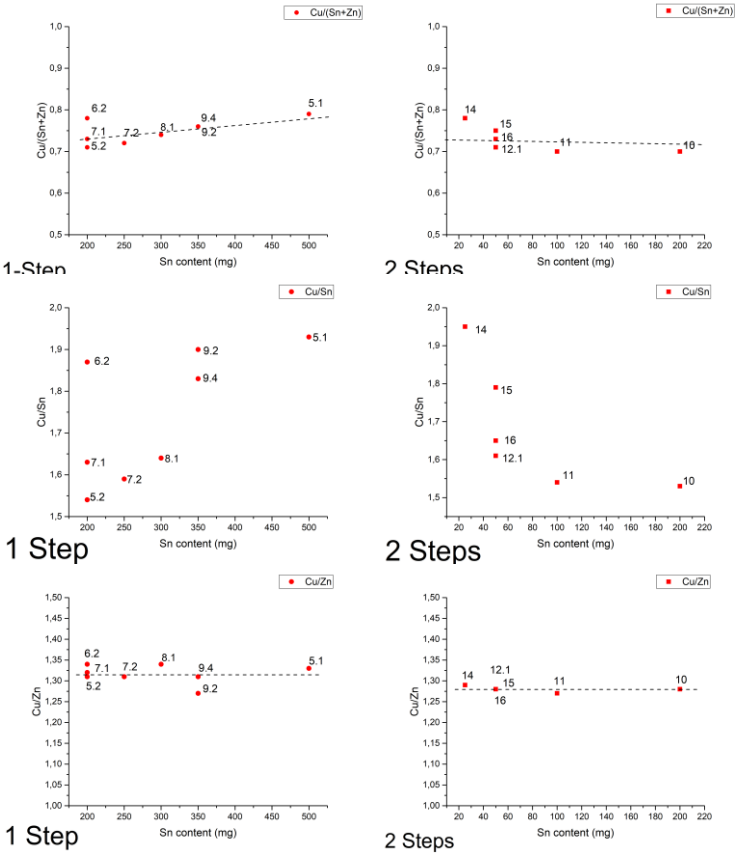

Figure 18: Compositional ratios of samples with different Sn content during annealing

In **Figure 19** we can see the results from the Raman spectroscopy. For M1 set of samples, samples 6.2 and 9.4 have a higher 169 cm^{-1} peak and a lower 243 cm^{-1} peak, while samples 5.2 and 10 have a lower 169 cm^{-1} peak, a higher 219 cm^{-1} peak, and a higher 243 cm^{-1} one. For the M2 set of samples, 7.2, 11 and 12.1 show very similar spectra, while samples 12.2 and 14 have a much higher 169 cm^{-1}peak and a lower 219 cm^{-1} peak. In addition, sample 14 has a very lower 243 cm^{-1} peak, but the difference is not so high for sample 12.2. All these observed peaks correspond to vibrational modes of the $Cu_2ZnSnSe_4$.

No secondary phases sensible to 785 nm excitation, such as Cu_2SnSe and Sn-Se compounds. In the case of the ZnSe phase, 442 nm excitation should be employed, but the presence of the CdS buffer layer prevents to use it, since any signal from the absorber would be hidden.

The relative intensity of the CZTSe Raman peaks has been related to the presence of point defects. In particular, a decrease of the 169 cm^{-1} peak indicates an increase of the copper vacancies (V_{Cu}), while an increase of the 243 cm^{-1} peak indicates an increase of the zinc-on-tin antisite (Zn_{Sn}) [51], [52]. So, samples 6.2, 9.4, and 14 have a lower presence of V_{Cu}, but similar Zn_{Sn} concentration than the rest of the samples. This is in agreement with the lower full width at half-maximum (FWHM) of the 192 cm^{-1} peaks observed for these samples, which indicates a better crystalline quality of the CZTSe phase.

It must be considered that the V_{Cu} concentration is associated to the minority carrier concentration, so the higher crystalline quality does not imply better optoelectronic parameters.

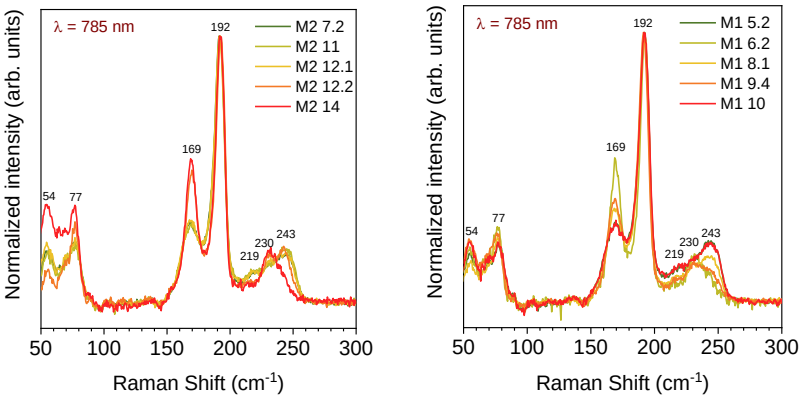

Figure 19: Raman spectra obtained using 785 nm excitation wavelength of different CZTSe samples synthesized from bronze-based precursor. On the left, M2 set of samples. On the right, M1 set of samples

Finally, of all the devices fabricated, it has only been possible to determine the optoelectronic parameters of four of them. In **Table 5** all the parameters obtained from the illuminated JV curve are summarized (the parameters were extracted from **Figure**

21). If we compare the V_{oc} measured in these devices (**Figure 21**) with the theoretical from Schokley-Queisser limit in **Figure 20**, we can see that not even 50% of the ideal value (~850mV) has been reached. This is enough evidence that the V_{oc} deficit problem has not been solved at all and is still the main challenge of this technology.

Table 5: Solar Cell Parameters extracted from the IV curves of the working devices.

Sample	J_{sc} (mA/cm²)	I_{sc} (mA)	V_{oc} (mV)	I_{mpp} (mA)	V_{mpp} (mV)	FF (%)	Eff (%)
5.2	30.68	2.67	358.62	1.96	231.01	47.34	5.21
10	25.07	2.18	322.58	1.42	201.45	40.8	3.30
12.1	31.68	2.76	365.49	2.12	245.75	51.63	5.98
12.2	32.04	2.78	330.12	2.05	216.24	48.39	5.11

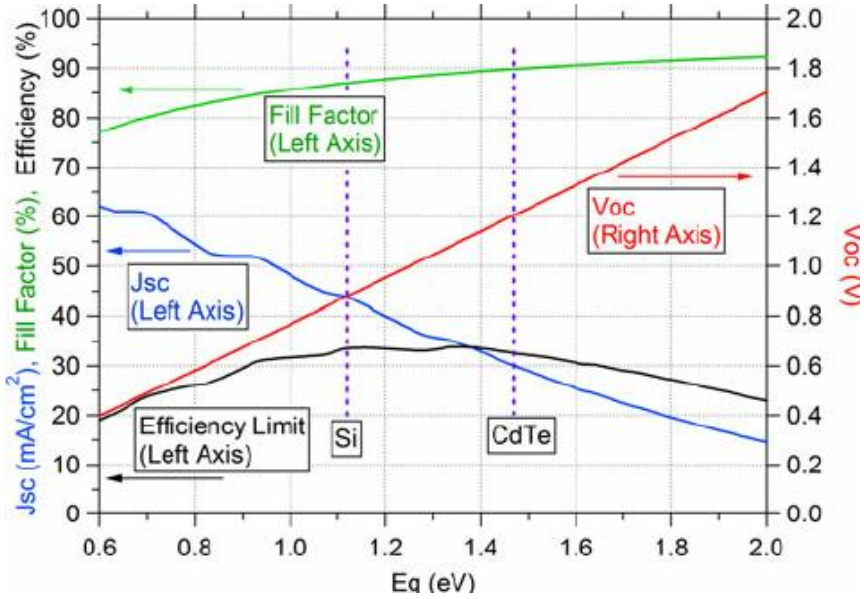

Figure 20: Schokley-Queisser Limit's V_{oc} depending on the bandgap of the material

In **Figure 21** the IV-curves of representative devices are represented. The results can be tentatively compared with Raman spectroscopy characterization. It was to be expected

a relatively good performance from samples 5.2 and 12.1 due to its low 169 cm^{-1} peak, that is relate to Cu-defects. In particular, a low intensity on this Raman mode indicates lower quantity of defects in the corresponding lattice plane, and is commonly associated with higher V_{oc}. In fact, samples 5.2 and 12.1 exhibit the highest V_{oc} among all the samples correlating well with this feature. On the other hand, it is impressive the behavior of samples 10 and 12.2 that, even presenting a high 169 cm^{-1}, have performed well compared to other samples. Nevertheless, these samples exhibit lower V_{oc} lower than 5.2 and 12.1 devices, probably due to higher Cu-related defects as observed by Raman. Even though, a more extensive characterization would be necessary in order to further explain the data obtained.

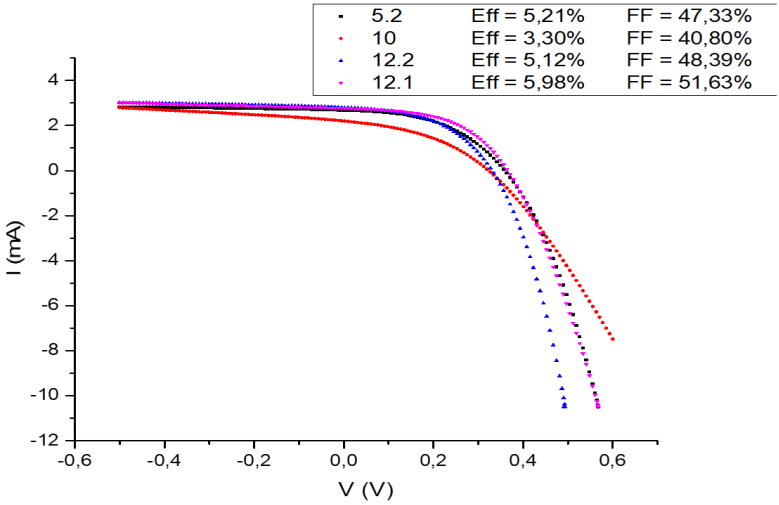

Figure 21: IV-Curves of the devices that showed a photoelectric response

8. CONCLUSIONS AND PERSPECTIVES

In this work we have studied selenization of Sn-poor precursors using one and two-steps reactive annealing processes. The main conclusions of this research are:

After several experiments, it was possible to obtain the appropriate composition for $Cu_2ZnSnSe_4$ absorbers, determined by XRF. It was shown that it is possible to use a Cu-rich Sn-poor target (Cu_3Sn), efficiently introducing Sn from the atmosphere during annealing and synthesize a Cu-poor absorber thanks to the compositional control of the reactive atmosphere.

It was determined that after a given Sn-quantity threshold, no matter how much more Sn is added to the reactive atmosphere, the final composition of the absorber will not be affected. The above is true for two-step processes, as the first process at a lower temperature is the responsible one for the Sn regulation in the CZTSe layer.

It was also determined that in order to obtain the needed composition the annealing must be done at low total pressures all the way.

Despite no secondary phases were detected in the Raman spectroscopy analysis (at least with 785 nm excitation wavelength) and the compositions weren't far from the ideal, many of the devices failed to work, and in some of them we obtain reasonably good conversion efficiencies. Unfortunately, with the characterization that could be done due to the current circumstances, not enough information is available to determine the main issues behind the possible introduction of Sn from the atmosphere in Sn-poor precursors. Superficial and cross-section SEM images would be a great help as well as XRD, XPS and Raman spectroscopy with other excitation wavelengths, and a deeper analysis of the solar cell devices, to further improve the reported efficiencies.

Although the results obtained are limited to drawn clear conclusions, some aspects can be highlighted for future research on this topic. There are many possibilities of improving kesterite performance by adding more elements to the structure, such as Ge,

but without a doubt the best discovery would be doing it just by optimizing the processes, since adding more elements implies an increase on the complexity of the material.

To finish, something that has not been seen in this work but has a good future is a low temperature-post annealing treatment (LT-PAT), commonly known as hot-plating. This treatment has been reported to increase performance of kesterite solar cells. Nevertheless, the results presented in this report demonstrate that the use of Sn-poor precursors and further regulation of Sn from the atmosphere is very promising, and merits deeper investigation in the future.

9. REFERENCES

[1] M. Kampa y E. Castanas, «Human health effects of air pollution», *Environmental Pollution*, vol. 151, n.º 2, pp. 362-367, ene. 2008, doi: 10.1016/j.envpol.2007.06.012.

[2] J. M. Gregory y J. Oerlemans, «Simulated future sea-level rise due to glacier melt based on regionally and seasonally resolved temperature changes», *Nature*, vol. 391, n.º 6666, pp. 474-476, ene. 1998, doi: 10.1038/35119.

[3] S. E. Schwartz, «Uncertainty in climate sensitivity: Causes, consequences, challenges», *Energy Environ. Sci.*, vol. 1, n.º 4, p. 430, 2008, doi: 10.1039/b810350j.

[4] J. M. Last, K. Trouton, D. Pengelly, y David Suzuki Foundation, *Taking our breath away: the health effects of air pollution and climate change*. Vancouver: David Suzuki Foundation, 1998.

[5] A. Allaby y M. Allaby, «A dictionary of earth sciences», en *A dictionary of earth science*, Oxford; New York : Oxford University Press, 1999, p. 258.

[6] M. Sato, «Thermochemistry of the formation of fossil fuels», p. 14.

[7] «BP Statistical Review of World Energy». 2019.

[8] J. Houghton, *Global Warming: The Complete Briefing*, 4.ª ed. CAMBRIDGE, 2009.

[9] «Renewable power generation costs in 2018», p. 88.

[10] A. M. Bradshaw, B. Reuter, y T. Hamacher, «The Potential Scarcity of Rare Elements for the Energiewende», *Green*, vol. 3, n.º 2, ene. 2013, doi: 10.1515/green-2013-0014.

[11] S. Bowden y C. Honsberg, «PV Education». https://www.pveducation.org/.

[12] I. Becerril-Romero, «Alternative substrates for sustainable and Earth-abundant thin film photovoltaics», Universitat de Barcelona, Barcelona, 2020.

[13] D. Yue, F. You, y S. B. Darling, «Domestic and overseas manufacturing scenarios of silicon-based photovoltaics: Life cycle energy and environmental comparative analysis», *Solar Energy*, vol. 105, pp. 669-678, jul. 2014, doi: 10.1016/j.solener.2014.04.008.

[14] W. Hermes, D. Waldmann, M. Agari, K. Schierle-Arndt, y P. Erk, «Emerging Thin-Film Photovoltaic Technologies», *Chemie Ingenieur Technik*, vol. 87, n.º 4, pp. 376-389, abr. 2015, doi: 10.1002/cite.201400101.

[15] S. Lee *et al.*, «*In Situ* Process to Form Passivated Tunneling Oxides for Front-Surface Field in Rear-Emitter Silicon Heterojunction Solar Cells», *ACS Sustainable Chem. Eng.*, vol. 7, n.º 24, pp. 19332-19337, dic. 2019, doi: 10.1021/acssuschemeng.9b05534.

[16] J. Benick *et al.*, «High-Efficiency n-Type HP mc Silicon Solar Cells», *IEEE J. Photovoltaics*, vol. 7, n.º 5, pp. 1171-1175, sep. 2017, doi: 10.1109/JPHOTOV.2017.2714139.

[17] T. Nishio *et al.*, «THIN-FILM CdS/CdTe SOLAR CELL WITH 15.05% EFF:ICIENCY», p. 4.

[18] R. Scheer y H.-W. Schock, *Chalcogenide Photovoltaics: Physics, Technologies, and Thin Film Devices*. Weinheim, Germany: Wiley-VCH Verlag GmbH & Co. KGaA, 2011.

[19] N.-G. Park, «Perovskite solar cells: an emerging photovoltaic technology», *Materials Today*, vol. 18, n.º 2, pp. 65-72, mar. 2015, doi: 10.1016/j.mattod.2014.07.007.

[20] J. Ajayan, D. Nirmal, P. Mohankumar, M. Saravanan, M. Jagadesh, y L. Arivazhagan, «A review of photovoltaic performance of organic/inorganic solar cells for future renewable and sustainable energy technologies», *Superlattices and Microstructures*, vol. 143, p. 106549, jul. 2020, doi: 10.1016/j.spmi.2020.106549.

[21] J. Li, D. Wang, X. Li, Y. Zeng, y Y. Zhang, «Cation Substitution in Earth-Abundant Kesterite Photovoltaic Materials», *Adv. Sci.*, vol. 5, n.º 4, p. 1700744, abr. 2018, doi: 10.1002/advs.201700744.

[22] S. Schorr, «The crystal structure of kesterite type compounds: A neutron and X-ray diffraction study», *Solar Energy Materials and Solar Cells*, vol. 95, n.º 6, pp. 1482-1488, jun. 2011, doi: 10.1016/j.solmat.2011.01.002.

[23] S. R. Hall, J.T. Szymanski, y J. M. Stewart, «KESTERITE AND STANNITE, STRUCTURALLY SIMILAR BUT DISTINCT MINERALS», p. 7.

[24] S. Chen, X. G. Gong, A. Walsh, y S.-H. Wei, «Crystal and electronic band structure of Cu2ZnSnX4 (X=S and Se) photovoltaic absorbers: First-principles insights», *Appl. Phys. Lett.*, vol. 94, n.º 4, p. 041903, ene. 2009, doi: 10.1063/1.3074499.

[25] X. Fontané *et al.*, «Vibrational properties of stannite and kesterite type compounds: Raman scattering analysis of Cu2(Fe,Zn)SnS4», *Journal of Alloys and Compounds*, vol. 539, pp. 190-194, oct. 2012, doi: 10.1016/j.jallcom.2012.06.042.

[26] J. J. S. Scragg, L. Choubrac, A. Lafond, T. Ericson, y C. Platzer-Björkman, «A low-temperature order-disorder transition in Cu_2ZnSnS_4 thin films», *Appl. Phys. Lett.*, vol. 104, n.º 4, p. 041911, ene. 2014, doi: 10.1063/1.4863685.

[27] G. Rey *et al.*, «The band gap of Cu2ZnSnSe4: Effect of order-disorder», *Appl. Phys. Lett.*, vol. 105, n.º 11, p. 112106, sep. 2014, doi: 10.1063/1.4896315.

[28] A. Fairbrother, M. Dimitrievska, Y. Sánchez, V. Izquierdo-Roca, A. Pérez-Rodríguez, y E. Saucedo, «Compositional paradigms in multinary compound systems for photovoltaic applications: a case study of kesterites», *J. Mater. Chem. A*, vol. 3, n.º 18, pp. 9451-9455, 2015, doi: 10.1039/C5TA02000J.

[29] M. Neuschitzer, «DEVELOPMENT OF CU2ZNSNSE4 BASED THIN FILM SOLAR CELLS BY PVD AND CHEMICAL BASED PROCESSES», p. 137.

[30] M. Grossberg *et al.*, «The electrical and optical properties of kesterites», *J. Phys. Energy*, vol. 1, n.º 4, p. 044002, ago. 2019, doi: 10.1088/2515-7655/ab29a0.

[31] C. J. Hages *et al.*, «Identifying the Real Minority Carrier Lifetime in Nonideal Semiconductors: A Case Study of Kesterite Materials», *Adv. Energy Mater.*, vol. 7, n.º 18, p. 1700167, sep. 2017, doi: 10.1002/aenm.201700167.

[32] L. Grenet, M. A. A. Suzon, F. Emieux, y F. Roux, «Analysis of Failure Modes in Kesterite Solar Cells», *ACS Appl. Energy Mater.*, vol. 1, n.º 5, pp. 2103-2113, may 2018, doi: 10.1021/acsaem.8b00194.

[33] S. R. Kodigala, «Cu(In1−xGax)Se2 and CuIn(Se1−xSx)2 Thin Film Solar Cells», en *Thin Films and Nanostructures*, vol. 35, Elsevier, 2010, pp. 505-679.

[34] S. Zamulko, K. Berland, y C. Persson, «Optical Properties of CZTSSe by First-Principles Calculations», *Phys. Status Solidi A*, vol. 215, n.º 17, p. 1700945, sep. 2018, doi: 10.1002/pssa.201700945.

[35] S. Lopez-Marino *et al.*, «The importance of back contact modification in Cu2ZnSnSe4 solar cells: The role of a thin MoO2 layer», *Nano Energy*, vol. 26, pp. 708-721, ago. 2016, doi: 10.1016/j.nanoen.2016.06.034.

[36] T. Ratz *et al.*, «Physical routes for the synthesis of kesterite», *J. Phys. Energy*, vol. 1, n.º 4, p. 042003, sep. 2019, doi: 10.1088/2515-7655/ab281c.

[37] A. Redinger, D. M. Berg, P. J. Dale, y S. Siebentritt, «The Consequences of Kesterite Equilibria for Efficient Solar Cells», *J. Am. Chem. Soc.*, vol. 133, n.º 10, pp. 3320-3323, mar. 2011, doi: 10.1021/ja111713g.

[38] Y. S. Lee *et al.*, «Cu2ZnSnSe4 Thin-Film Solar Cells by Thermal Co-evaporation with 11.6% Efficiency and Improved Minority Carrier Diffusion Length», *Adv. Energy Mater.*, vol. 5, n.º 7, p. 1401372, abr. 2015, doi: 10.1002/aenm.201401372.

[39] A. V. Moholkar *et al.*, «Development of CZTS thin films solar cells by pulsed laser deposition: Influence of pulse repetition rate», *Solar Energy*, vol. 85, n.º 7, pp. 1354-1363, jul. 2011, doi: 10.1016/j.solener.2011.03.017.

[40] J. Schou *et al.*, «Pulsed laser deposition of chalcogenide sulfides from multi- and single-component targets: the non-stoichiometric material transfer», *Appl. Phys. A*, vol. 124, n.º 1, p. 78, ene. 2018, doi: 10.1007/s00339-017-1475-3.

[41] A. Cazzaniga *et al.*, «Ultra-thin Cu2ZnSnS4 solar cell by pulsed laser deposition», *Solar Energy Materials and Solar Cells*, vol. 166, pp. 91-99, jul. 2017, doi: 10.1016/j.solmat.2017.03.002.

[42] M. T. Winkler, W. Wang, O. Gunawan, H. J. Hovel, T. K. Todorov, y D. B. Mitzi, «Optical designs that improve the efficiency of Cu2ZnSn(S,Se)4 solar cells», *Energy Environ. Sci.*, vol. 7, n.º 3, pp. 1029-1036, 2014, doi: 10.1039/C3EE42541J.

[43] H. Xin, J. K. Katahara, I. L. Braly, y H. W. Hillhouse, «8% Efficient Cu2ZnSn(S,Se)4 Solar Cells from Redox Equilibrated Simple Precursors in DMSO», *Adv. Energy Mater.*, vol. 4, n.º 11, p. 1301823, ago. 2014, doi: 10.1002/aenm.201301823.

[44] T. Todorov *et al.*, «Solution-based synthesis of kesterite thin film semiconductors», *J. Phys. Energy*, vol. 2, n.º 1, p. 012003, ene. 2020, doi: 10.1088/2515-7655/ab3a81.

[45] F. C. Krebs, «Fabrication and processing of polymer solar cells: A review of printing and coating techniques», *Solar Energy Materials and Solar Cells*, vol. 93, n.º 4, pp. 394-412, abr. 2009, doi: 10.1016/j.solmat.2008.10.004.

[46] E. Saucedo *et al.*, «Driving the kesterite formation pathway with the chalcogen availability: a kinetic and phase analysis», nov. 2019.

[47] S. Schorr *et al.*, «Point defects, compositional fluctuations, and secondary phases in non-stoichiometric kesterites», *J. Phys. Energy*, vol. 2, n.º 1, p. 012002, dic. 2019, doi: 10.1088/2515-7655/ab4a25.

[48] S. López-Marino *et al.*, «ZnSe Etching of Zn-Rich Cu2ZnSnSe4: An Oxidation Route for Improved Solar-Cell Efficiency», *Chem. Eur. J.*, vol. 19, n.º 44, pp. 14814-14822, oct. 2013, doi: 10.1002/chem.201302589.

[49] H. Xie *et al.*, «Impact of Sn(S,Se) Secondary Phases in Cu2ZnSn(S,Se)4 Solar Cells: a Chemical Route for Their Selective Removal and Absorber Surface Passivation», *ACS Appl. Mater. Interfaces*, vol. 6, n.º 15, pp. 12744-12751, ago. 2014, doi: 10.1021/am502609c.

[50] Y. Sanchez, «Síntesis química de capas buffer para nuevas tecnologías de calcogenuros con aplicaciones fotovoltaicas.», Universitat de Barcelona, Barcelona, 2019.

[51] M. Guc, S. Levcenko, V. Izquierdo-Roca, X. Fontané, E. Arushanov, y A. Pérez-Rodríguez, «Polarized Raman scattering analysis of $Cu_2ZnSnSe_4$ and $Cu_2ZnGeSe_4$ single crystals», *Journal of Applied Physics*, vol. 114, n.º 19, p. 193514, nov. 2013, doi: 10.1063/1.4830028.

[52] M. Dimitrievska, A. Fairbrother, E. Saucedo, A. Pérez-Rodríguez, y V. Izquierdo-Roca, «Influence of compositionally induced defects on the vibrational properties of device grade $Cu_2ZnSnSe_4$ absorbers for kesterite based solar cells», *Appl. Phys. Lett.*, vol. 106, n.º 7, p. 073903, feb. 2015, doi: 10.1063/1.4913262.